The Effect of Heat Input on the Microstructure and Properties of Nickel Aluminum Bronze Laser Clad with a Consumable of Composition Cu-9.0Al-4.6Ni-3.9Fe-1.2Mn

C.V. HYATT, K.H. MAGEE and T. BETANCOURT

The effect of heat input in the laser cladding of nickel aluminum bronze was investigated. Nickel aluminum bronze castings were clad with a consumable of the composition Cu-9.0Al-4.6Ni-3.9Fe-1.2Mn and exposed to a variety of heat inputs from 42.5 to 595 J/mm. At the lowest heat input, the deposit microstructure was almost entirely martensitic. Increases in heat input caused the amount of α to increase. Depending upon heat input, the α was present as grain boundary allotriomorphs, secondary Widmanstätten α sideplates, and intragranular Widmanstätten α precipitates. The reheated zones were of lower hardness and, at all heat inputs, consisted of a mixture of grain boundary allotriomorphs and Widmanstätten α and martensite. Laser cladding improved the corrosion- and cavitation-erosion resistance of the surfaces but reduced their ductility. The properties of the clad surfaces depended on heat input.

I. INTRODUCTION

Laser cladding with nickel aluminum bronze offers the promise of order-of-magnitude improvements in the surface-sensitive properties of nickel aluminum bronzes and other alloys. It is also a promising repair and reclamation method for high-value components. Cladding of nickel aluminum bronze castings with nickel aluminum bronze is of particular interest in marine engineering applications. Here, the development of seawater handling, propulsion, and combat system equipment capable of lasting the life of a ship would offer enormous cost benefits. Nickel aluminum bronzes are selected for use in high-performance marine engineering applications for their ease of fabrication by casting, welding, and forging and for their properties.[1,2] Their resistance to corrosion, erosion-corrosion, cavitation-erosion, corrosion-fatigue, stress corrosion cracking, and dealloying are particularly important. So are their toughness and strength. These properties impose limitations on the design, use, and life of components made of nickel aluminum bronze. For example, the design guidelines for propellers made of nickel aluminum bronze are basically limited by corrosion fatigue,[2,3,4] the life and inspection intervals of nickel aluminum bronze valves in seawater handling systems are limited by dealloying,[5–8] and the damage of nickel aluminum bronze impellers and propellers by cavitation-erosion does occur. Improvements in these properties, without degradation of others, could give significant cost and performance benefits.

It has been known for some time that the properties of aluminum bronzes can be modified by solid-state quenching[9] and by rapid solidification and laser surface melting.[10–16] Because the intermetallic compounds in nickel aluminum bronzes are very stable and the α-β phase boundary is near the solidus line, it is very difficult to homogenize these alloys in the solid state.[9,17] Thus, a welding approach is required.

There exists information on the development of microstructures in low-heat-input welding of nickel aluminum bronze.[18–29] Except for some weld simulation studies,[29] all this work has dealt with alloys rich enough in aluminum that martensite can be produced following rapid quenching from the melt. For the alloys examined thus far, in the as-deposited material, a martensite with a 9-R structure is common in low-heat-input nickel aluminum bronze welds over a range of compositions. Other phases, identified by various workers as Widmanstätten α, bainite, or lath martensite, also form. Weld simulation data also show that, for at least one alloy composition, formation of Widmanstätten α can be suppressed with a high enough cooling rate ($\Delta t_{800°C-500°C}$ of 0.1 seconds or faster). As well, data show that tempering of martensites in weld-reheated and heat-affected zones probably does not occur at temperatures of less than roughly 400 °C.[9,30] Transmission electron microscopy studies, to be published shortly, suggest that, within the reheated zones between passes, the structure consists of a mixture of faulted 9-R–type martensite and coarsened, light-etching Widmanstätten plates.[18,19,25,27,31] It has also been shown that the prior wrought or cast structure plays a significant role in the heat-affected zone microstructure. For example, within the heat-affected zone, partial dissolution and transformation of prior intermetallics occurs.[23,24,27,28] A more complete review of microstructural transformations related to low-heat-input welding of nickel aluminum bronze is given elsewhere, but a greater understanding is required.[31]

Previous work on laser cladding of nickel aluminum bronzes, especially in heat-input regimes useful in engineering practice, has dealt mostly with microstructural characterization. Data on properties and on the relationship between processing conditions, microstructure, and properties are lacking. As well, the data that are available have been accumulated on a number of different alloys, using a

C.V. HYATT, Defence Scientist, is with Defence Research Establishment Atlantic, Dartmouth, NS, Canada B2Y 3Z7. K.H. MAGEE, formerly Metallurgical Engineer with The Laser Institute, Edmonton, AB, Canada T6E 5J1, is Senior Metallurgical Engineer with CANSPEC Group Inc., Edmonton, AB, Canada T6P 1N8. T. BETANCOURT, formerly Corrosion Scientist with the Nova Scotia Innovation Corp., Dartmouth, NS, Canada B2Y 3Z7, is retired.

Manuscript submitted August 29, 1997.

REPRODUCED BY PERMISSION
OF THE MINISTER OF SUPPLY AND SERVICES CANADA

Table I. Compositions, Dimensions, and Uses of Coupons

Alloy	Designation (UNS)	Thickness (mm)	Specimen Composition				
			Cu	Al	Ni	Fe	Mn
A	C95800	~25	80.3	8.75	4.8	4.4	1.4
B	C95800	~25	81.1	8.63	4.8	4.0	1.1
C	C95800*	[illegible]	79.3	9	4.3	4.9	0.86
W (wire)	(ER) CuNiAl	0.25, 0.89 (diameter)	80.8	9.0	4.6	3.9	1.2

*The material was supplied with this designation. Because iron is greater than nickel, it does not satisfy the chemical analysis requirements.

Table II. Cladding Conditions for Specimens Used in This Work

Type of Specimen	Base Alloy	Laser Power (W)	Travel Speed (mm/s)	Wire Diameter (mm)	Defocus (mm)	Number of Layers	Shielding Gas	Heat Input (J/mm)
C43/1	C	1800	42	0.25	—	1	helium	42.5
C47/1	C	1800	38	0.25	—	1	helium	47.2
C64/2	C	2700	42	0.25	6.4	2	helium	64.3
C64/3	C	2700	42	0.25	6.4	3	helium	64.3
C595/2	C	5000	8.4	0.89	12	2	helium	595
A390/1	A or B	4100	10.6	0.25	12	1	argon	390
A68/1	A or B	2900	42	0.25	7.6	1	argon	68.0
A150/1	A or B	3300	21	0.25	10.2	1	argon	150
A150/2	A or B	3300	21	0.25	10.2	2	argon	150
A150/3	A or B	3300	21	0.25	10.2	3	argon	150

range of different processes and welding geometries. This makes comparisons difficult. This article overcomes the shortcomings just mentioned by examining the effect of processing conditions in laser cladding on the microstructure and properties of nickel aluminum bronze. One composition of commercially available ErCuNiAl weld wire was used to clad UNS C95000 castings typical of those used in marine engineering applications. Heat inputs from 42.5 to 595 J/mm were used, and a number of significant properties were investigated.

II. MATERIALS AND METHODS

A. *Castings and Consumables*

The materials used in this study included cast coupons meeting UNS C95800 and ErCuNiAl weld wire. Several different sizes and compositions of coupons were used. These are summarized in Table I. Pretreatment of the coupons prior to welding involved machining them flat, glass bead blasting, washing with a soft bristle brush and soapy water, and degreasing with acetone.

B. *Laser Cladding*

The cladding experiments were done with a 5 kW CO_2 laser equipped with two different arrangements to feed the wire to the deposit. One arrangement used 0.89-mm wire and the other arrangement used 0.25-mm wire. The arrangement used to feed and position the 0.89-mm-diameter wire consisted of a gas metal arc welding torch attached to a commercial wire feeder. Argon or helium shielding was provided through orifices in the torch tip in the normal way. In the arrangement used to feed the 0.25-mm-diameter wire, the gas metal arc welding torch was replaced with the tip of a hypodermic needle connected to a custom-built wire feeder based on a stepper motor. Precise positioning of the needle tip was possible because it was mounted on a micrometer stage. With the fine wire arrangement, shielding gas was directed at the specimen surface through the primary gas nozzle attached to the laser optics head.

A number of process variables were adjusted by trial and error to produce the best-appearing deposit. For both wire sizes, wire was fed from the leading edge of the melt at an angle of 30 deg to the specimen surface. In the 0.89-mm wire arrangement, the specimen surface at the start of cladding was located at a position 11.9 mm beyond the focal point and the wire was aimed at the front of the melt pool. In the 0.25-mm wire arrangement, the specimen surface was located at a position 6.4 mm beyond the focal point and the wire was aimed to intersect the specimen surface about 1 mm in front of the melt pool. Information on the processing conditions used to produce each type of specimen examined in this work is given in Table II.

More details of the development of the laser welding procedures and their applications to the cladding of complex parts will be given in a future report.[32]

C. *Evaluation Procedures*

1. *Potentiodynamic corrosion studies*

Corrosion behavior was assessed on specimens of as-received alloy A and specimens of alloy A clad with heat inputs of 68 and 390 J/mm, respectively. The three as-received specimens examined were ground to a 600-grit finish. For each cladding condition, the specimens examined were tested in the as-clad condition. Immediately prior to testing, all specimens were washed in distilled water and degreased in acetone. The test system was calibrated according to the requirements of ASTM standard G5.[33] Tests were done with a three-electrode system using natural seawater at 25 °C which had been purged with nitrogen gas.

Corrosion potentials were determined after equilibrating the test specimens for 1 hour. During the polarization tests, voltage was applied continuously from open circuit potential to 1.1 V at a rate of 0.1 mV/s.

2. *Cavitation-erosion experiments*

Cavitation-erosion experiments were carried out according to ASTM standard G-32.[34] The test setup consisted of a piezoelectric vibrator unit equipped with a 12.7-mm-diameter horn to which a specimen was attached. Duplicate test specimens were machined from material clad with single layers at heat inputs of 68 and 390 J/mm and from unclad material. The test surface of each test specimen was ground to a 600-grit finish, and the specimen was washed in water and then in ethanol in an ultrasonic bath. Following air drying, the specimen was weighed to within ±0.1 mg. The test specimen, mounted on the horn of the ultrasonic unit, was immersed in 1.5 L of seawater at 25 ± 2 °C and oscillated at a frequency of 20 ± 0.5 kHz and at an amplitude of 50 μm. Periodically, the experiment was interrupted and the specimen was removed, cleaned, and weighed so that mass loss as a function of time could be determined. The performance of the test setup was shown to meet the requirements of ASTM standard G-32 by running a test with annealed nickel 200 in distilled water at 20 °C. To ensure consistency, prior to each seawater test, the seawater was sonicated with a Ni 200 specimen for 30 minutes to stabilize the gas content of the water. Calculation of the incubation time was obtained by extrapolating a tangent from the steepest linear section of the erosion-time curve to the time axis. This intersection with the time axis was taken as the incubation time.

3. *Long-term corrosion behavior*

To examine long-term corrosion behavior, the specimens listed in Table III were immersed in a tank through which Halifax Harbor seawater flowed. The specimens were immersed for a period of 5 months. Using data from References 5, 7, and 8, this time meets the requirements of ASTM G-4[35] for a valid immersion corrosion test. Specimens were 12.4 × 12.4 × 4 mm thick and had a 2.9-mm-diameter mounting hole drilled through them. The specimens were mounted on a 6-mm-thick sheet of polyacetal using nylon screws. Nylon nuts beneath the specimens allowed them to be spaced 1.5 cm away from the board. The head of the screw and the nylon nut beneath the specimen created small crevices on the specimen. Crevices were deliberately included on some specimens by putting a polyacetal plate the size of the specimen over the surface of the specimen. Previous researchers have shown that coupling nickel aluminum bronze to titanium alloys produces one of the worst galvanic conditions seen in practice.[5,7] Thus, a number of specimens were screwed to a block of Ti-6Al-4V with dimensions of 12.5 × 37.5 × 4 mm. The area of the Ti alloy block was more than 6 times the area of the specimens. In most cases, the clad faces (only one face was clad) faced up. The exceptions were a few cases where a clad face was coupled with its face toward a Ti alloy block.

4. *Bend tests*

The ductility of a typical laser-clad specimen was assessed by performing bend tests according to ASTM standard E 290-87.[36] Specimens for bend testing had dimensions of 76.2 × 4.8 × 1.56 mm. The specimens were entirely clad on one 76.2 × 4.8-mm face. The direction of welding was along the length of the specimens. For reasons of material availability, only specimens of type Al50/2 were investigated. In the tests, one end of the specimen was clamped in a vice against a bend die and the specimen was bent slowly around the die using stout leather as a backing. The test was viewed to be a success if the specimen bent completely around the bend die without the occurrence of cracking detectable by dye-penetrant inspection. The purpose of the testing was to compare the ductility of the clad material to that of the base material. Thus, half the specimens were tested with the clad faces toward the face of the die and half were tested with the clad faces away from the face of the die.

5. *Stress corrosion cracking behavior*

Stress corrosion cracking tests were performed using specimens like those described in References 37 and 38 and shown in Figure 1. These "tuning-fork specimens" allowed the stresses to be estimated on the nonlaser-clad face from strain gage records collected from a dummy specimen. Three types of specimens were used. All had been laser clad with two layers on one outer face with a heat input of 150 J/mm (specimen type Al50/2). One type of specimen had an as–laser-clad finish. A second type was finished by grinding on metallographic papers to a 600-grit finish. A third type was similarly ground but contained defects in the region of high stress. These defects were either surface-breaking porosity, caused by the interaction of the laser-clad deposit with prior casting defects, or scribe lines. Stresses between 60 pct of the yield strength and 140 pct of the ultimate strength of the base material were induced by closing the tines of the tuning-fork specimens. Stresses were estimated from a relationship between surface strain and opening of the tines, determined by strain gaging the material on the unclad tine. Specimens were immersed in flowing Halifax Harbor seawater. Three specimens were removed after 1 month and six more were removed after 6 months, the last month of which was spent in stagnant Halifax Harbor seawater due to a seawater system failure.

III. RESULTS

A. *Metallography*

Low-magnification optical micrographs of specimens prepared by cladding with multiple layers are shown in Figure 2, while low-magnification optical micrographs of specimens prepared by cladding with single layers are shown in Figure 3. In both cases, microhardnesses measured on the specimens are also shown graphically. In this article, only the structures of the as-deposited and reheated weld metal are discussed. The reasons for this simplification are that the structure of the base casting has a large effect on the nature of the heat-affected zone and that, in the experiments on properties, it is the properties of the deposit, not those of the base metal heat-affected zone, which are being investigated.

Before proceeding to discuss the results, it is necessary to explain the difference in the thickness of deposit on the A and C series alloys and to comment on the significance of this to the development of microstructure. The C series specimens were clad using a helium gas shield, while the

Table III. Specimens Used in Dealloying Experiments

Specimen Origin	Coupling and Crevices	Preimmersion Weight (g)	Postimmersion Weight (g)	Weight Loss (g)	Metallographic Observations—Depth of Pitting
C(UT)	none	3.6851	3.6839	0.0012	20 μm
C64/2	none	4.1290	4.1262	0.0028	most >15 μm, one 60 μm
A150/2	none	3.5135	3.5111	0.0024	15 μm
A390/1	none	4.0699	4.0677	0.0022	20 μm
A(UT)	none	3.6830	3.6807	0.0023	100 μm
A(UT)	none	3.7468	3.7426	0.0042	40 μm
A(UT)	none	3.7834	3.7805	0.0029	30 μm
A(UT)	to Ti	4.2973	4.2936	0.0037	100 μm
A(UT)	to Ti	3.7861	3.7802	0.0059	100 μm
A150/2	to Ti	3.14842	3.4814	0.0028	15 μm
A150/2	coupled clad face down to Ti	3.3646	3.3598	0.0048	10 μm
A(UT)	nylon block covering upper surface	4.2736	4.2719	0.0017	20 μm
A150/2	nylon block covering clad surface	3.5866	3.5849	0.0017	10 μm

A series specimens were clad using an argon gas shield. For reasons to be discussed in another article, this allowed larger amounts of material to be deposited on the C series specimens than on the A series specimens.[32] For the purposes of this article, it is significant that differences in microstructures and microhardnesses in specimens, resulting from different amounts of dilution in specimens produced by cladding with either different deposition rates or different numbers of passes, appear to be minimal. This is based on the occurrence of similar hardnesses and microstructures in single and multipass welds and in welds produced at the same heat input but with different deposition rates. This probably occurs because the composition of the castings is similar to that of the weld deposit, and minimal dilution is expected. More significant dilution effects are observed when dissimilar substrates are clad.[32]

Significant changes in hardness occurred with increases in heat input. As shown in Figure 4, peak deposit hardness increased to a maximum Vickers hardness (HV) of 540 at a heat input of about 64 J/mm. The peak deposit hardness dropped after this. In contrast, as the graphs in Figures 2 and 3 show, the lowest hardness in the reheated zones was between 200 and 260 HV regardless of heat input.

Optical micrographs of the as-deposited material are shown in Figure 5. Those of the corresponding reheated zones are shown in Figure 6. Etching with 5 g $FeCl_3$ and 15 mL of HCl, dissolved in 60 mL of ethanol revealed a darker etching phase and a lighter etching phase. The lighter etching phase occurred as grain boundary allotriomorphs and also, sometimes, throughout grains, with a Widmanstätten morphology. The darker etching phase became progressively easier to etch on specimens produced with increasing heat input and showed more internal detail. We believe the white etching phase to be the α phase solid solution, which is stable in these alloys at low temperatures, and in this article we will call it the α phase. Designating the dark etching phase is more difficult. It certainly contains some martensite. However, it has been suggested that, at least at a few heat inputs, it also contains some bainitic

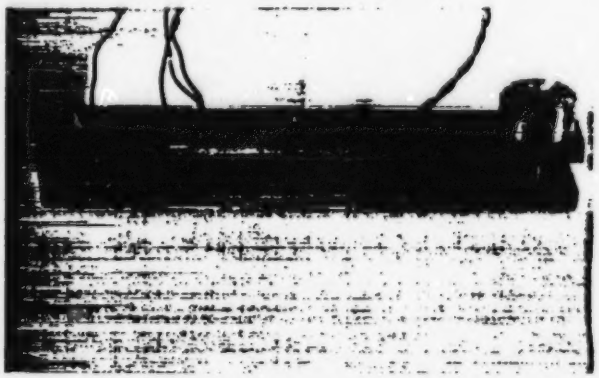

Fig. 1—Tuning fork-type stress corrosion specimen.

products as well as the products of autotempering.[31] Thus, for this article, we will designate the dark etching phase as the martensitic phase, realizing that the actual structures may be more complex in some cases. It is significant to note that we are not the first to encounter this difficulty. Workers who deal with solid-state transformations in nickel aluminum bronzes have often used the terminology β^* to describe all metastable β transformation products from quenching. Because the transformation products being considered here may be different than the solid-state ones, we have chosen not to adopt this convention.

The as-deposited material changed with heat input. At the lowest heat input investigated, 42.5 J/mm (Figure 5(a)), most of the as-deposited material seemed to be martensite. Only a small amount of grain boundary α formed. At a heat input of about 47.2 J/mm (Figure 5(b)), more than half the prior β grain boundaries had grain boundary allotriomorphs of α on them. As well, secondary Widmanstätten sideplates formed on many of the prior β grain boundaries upon which grain boundary allotriomorphs of α had formed. Deposits produced with a heat input of 64.3 J/mm

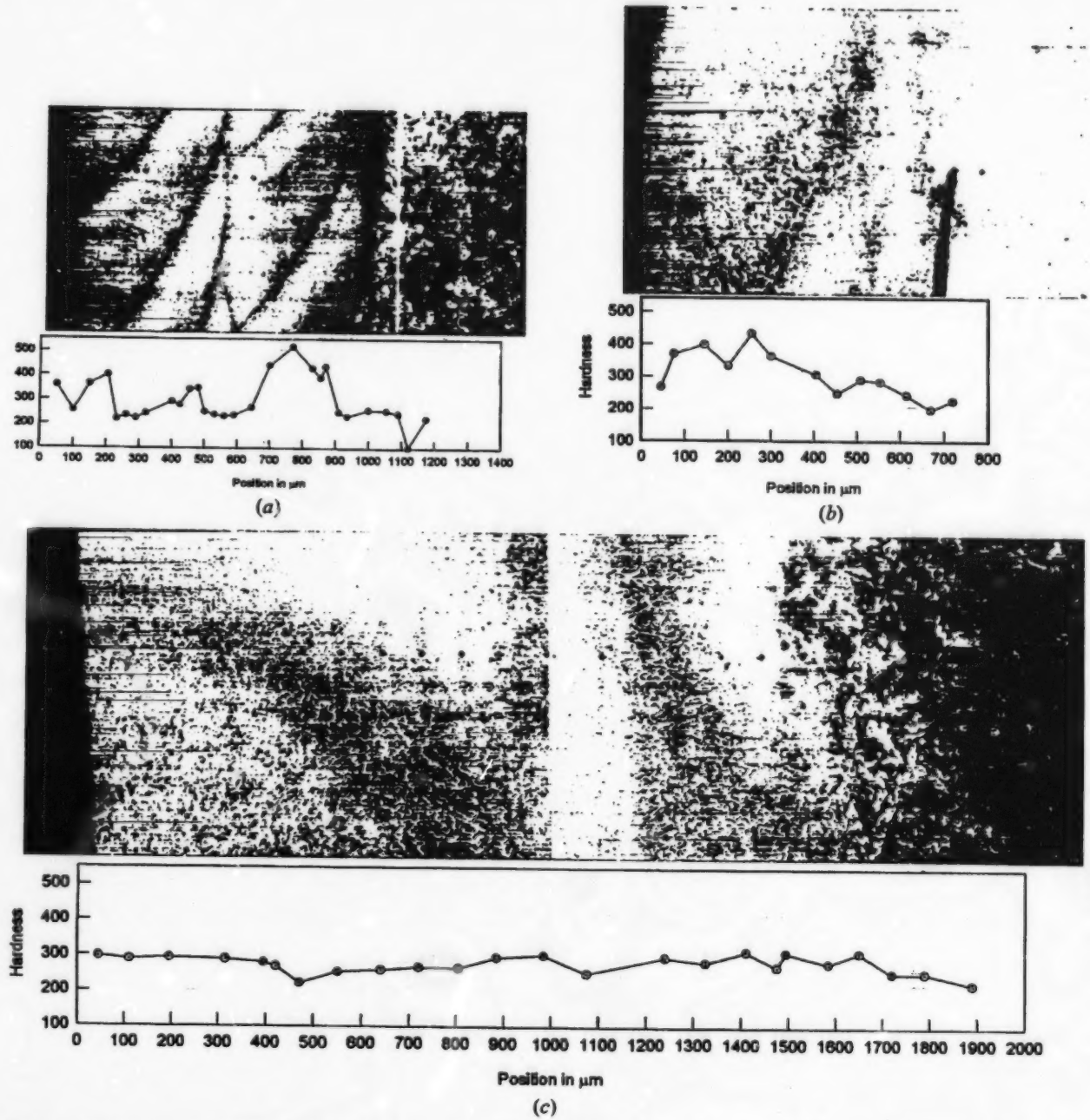

Fig. 2—Optical micrographs and microhardness scans on specimens clad with multiple passes: (*a*) specimen of type C64/3 (64.3 J/mm); (*b*) specimen of type A150/2 (150 J/mm); and (*c*) specimen of type C595/2 (595 J/mm).

(Figure 5(c)) had grain boundary allotriomorphs of α on most prior β grain boundaries. As with the 47.2 J/mm case, secondary Widmanstätten α sideplates formed on many of the prior β grain boundaries upon which grain boundary α had formed. Deposits produced at a heat input of 150 J/mm (Figure 5(d)) had all prior β grain boundaries outlined with α. Secondary Widmanstätten sideplates were pronounced, and some intragranular Widmanstätten precipitation of α may have occurred, although a darker-etching martensitic phase is still present. A deposit produced with a heat input of 390 J/mm was similar, although the volume fraction of α seems to have increased, primarily by the formation of what appears to be intragranular Widmanstätten plates and increased secondary Widmanstätten plate formation. The highest heat input investigated in this work, 595 J/mm, produced a microstructure with a similar volume fraction of

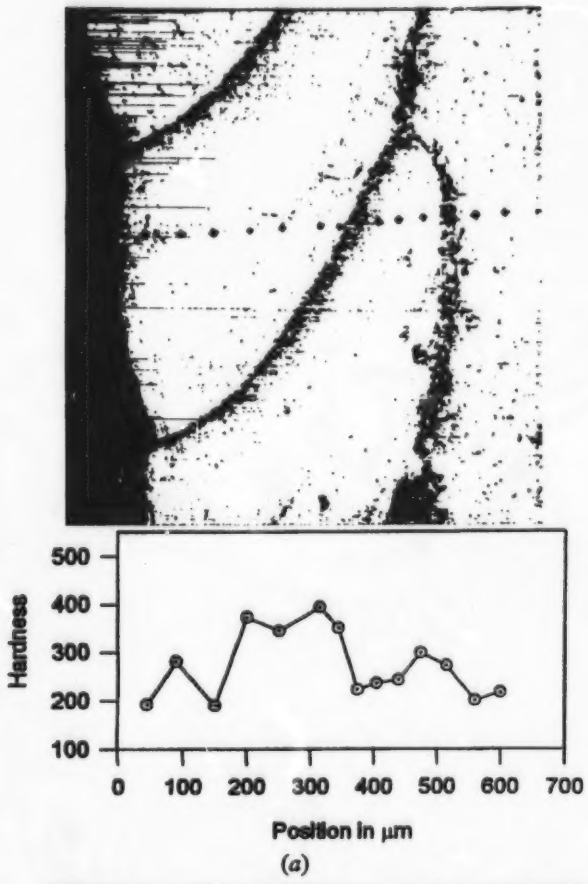

(a)

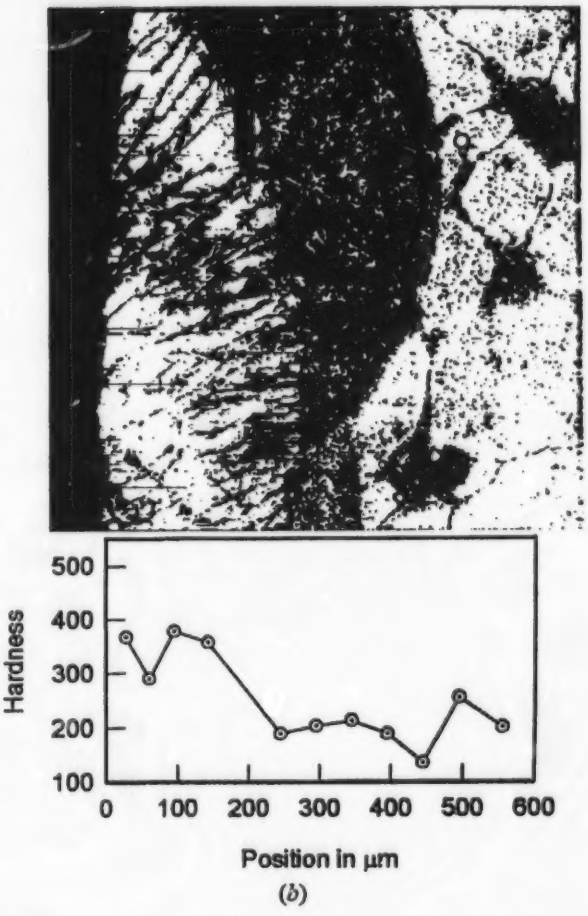

(b)

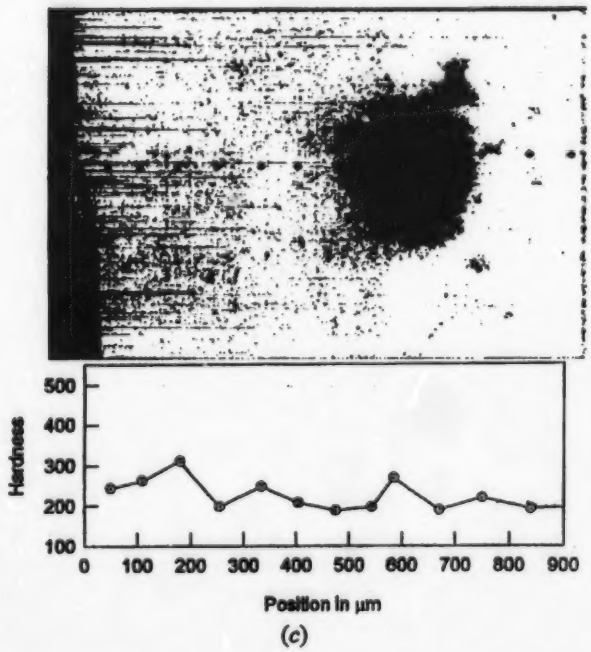

(c)

Fig. 3—Optical micrographs and microhardness scans on specimens clad with single passes: (*a*) specimen of type C47/1 (47 J/mm); (*b*) specimen of type A68/1 (68 J/mm), and (*c*) specimen of type A 390/1 (390 J/mm). Note the specimens shown in Figs. 3(b) and (c) had been subjected to cavitation erosion prior to sectioning.

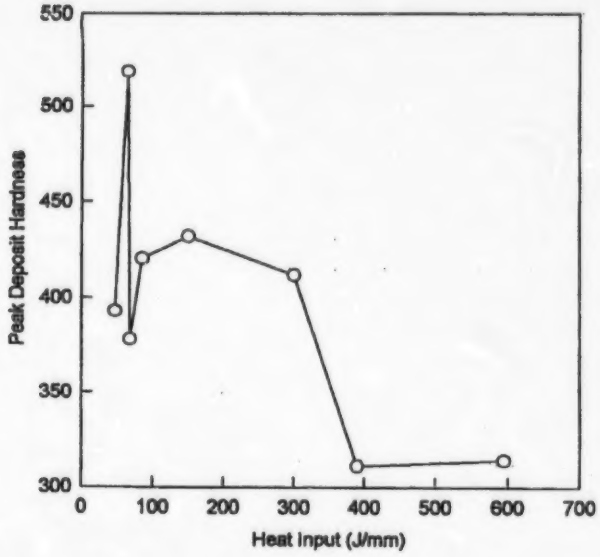

Fig. 4—Peak deposit hardness as a function of heat input.

martensite to the 390 J/mm case. The 595 J/mm heat input did seem to produce more intragranular Widmanstätten plates.

Compared to the as-deposited material, and except for the size of the zone, the reheated zone seemed to change less with heat input. This might have been expected from the relatively similar minimum reheated zone hardnesses. In this article, we consider only the coarsest part of the reheated zone. The reheated zones corresponding to the as-deposited materials just discussed are shown in Figure 6. In the reheated zones, for all heat inputs, the prior β grain boundaries are completely covered with grain boundary allotriomorphic α. Also, in all cases, there is some secondary Widmanstätten plate formation and extensive formation of what could be described as a basketweave pattern of (probably intragranular) Widmanstätten α.[29] From Figure 6, it is apparent that the main change in the reheated zone with increasing heat input is an increase in coarseness. It is also interesting that, at the two highest heat inputs examined (390 J/mm, Figure 6(e), and 595 J/mm, Figure 6(f)), a clearly equiaxed two-phase α plus β zone has developed in the reheated zone adjacent to the fusion line.

B. *Potentiodynamic Corrosion Behavior*

The results of the corrosion experiments are summarized in Table IV and Figure 7. As shown in Table IV, the corrosion potential of each specimen type was similar and typical of most copper alloys.[2] Grinding the surface of the clad specimens to a 600-grit finish did not significantly change the corrosion potential from that of the as-clad condition. Polarization curves are shown in Figure 7. Pitting, as suggested by the instability in current on one of the polarization curves for the 390 J/mm–clad specimens (Figure 7(b)) and confirmed by examination of this specimen, did occur on one of the 390 J/mm specimens. Grain boundary attack occurred on the as-received material. The corrosion current was estimated by extrapolating the anodic curve to the open circuit potential. Values of the corrosion current, which are proportional to the corrosion rate, are given in Table IV. These results suggest that specimens clad with a heat input of 68 J/mm will corrode about 10 times more slowly than the as-received material.

C. *Cavitation-Erosion Resistance*

The results of the cavitation-erosion experiments are shown in Figure 8. This figure shows the mean depth of erosion for laser-clad material produced with a low heat input (68 J/mm), clad material produced with a high heat input (390 J/mm), and that for the base material. The maximum cavitation-erosion rate and the incubation times for the three types of specimens tested are shown in Table V. The results reveal that the resistance to cavitation-erosion (based on maximum erosion rate) was increased by a factor of 5 by laser cladding with a heat input of 68 J/mm and by a factor of 2.5 by laser cladding with a heat input of 390 J/mm. They also show that low-heat-input cladding with a heat input of 68 J/mm doubles the incubation time, while high-heat-input cladding has no effect on incubation time relative to that of the bulk material.

Sectioning of the cavitation-erosion specimens showed that attack was fairly extensive on the base alloy (Figure 9(a)), but was concentrated at the heat-affected zones of the clad specimens (Figures 9(b) and (c)). The higher-heat-input specimen (A390/1—Figure 9(b)) was affected more severely than the lower-heat-input specimen (A68/1—Figure 9(c)). This may be primarily due to hardness effects, but might also be affected by a change in the nature and density of Widmanstätten plate boundaries. A similar effect has been reported to affect the toughness of microstructurally similar Ti alloys.[29] The presence of crack-stopping plate-type boundaries in the clad specimens may explain why cracks running perpendicular to the surface occurred in the unclad material (refer to the arrow in Figure 9(a)) but did not occur in the clad specimen. It is also interesting to note that, on the low-heat-input specimen, cavitation damage seems to have occurred more deeply at and around prior β boundaries, most of which were covered with grain boundary allotriomorphic α (refer to the arrow in Figure 9(c)).

D. *Long-Term Corrosion Behavior*

The long-term corrosion specimens were coated with marine growth after removal from the immersion tanks. This heavy coating of marine growth is thought to have produced a fairly severe seawater corrosion environment. The results of these experiments, presented in terms of weight loss and maximum depth of pitting or preferential attack, are summarized in Table III. Weight loss data provide limited insight because only one face of the specimens was clad. Except for very local effects less than 10 μm deep on the treated and untreated alloy C, there was little evidence of dealloying, except on a few specimens which had developed a coppery surface hue. Thus, discussion of dealloying effects will need to be deferred until specimens immersed for a longer term can be examined.

The clad specimens which were exposed in the uncoupled condition without a nylon crevice all exhibited minor pitting in the as-deposited material. Similar results were observed on specimens exposed coupled to Ti. A severe

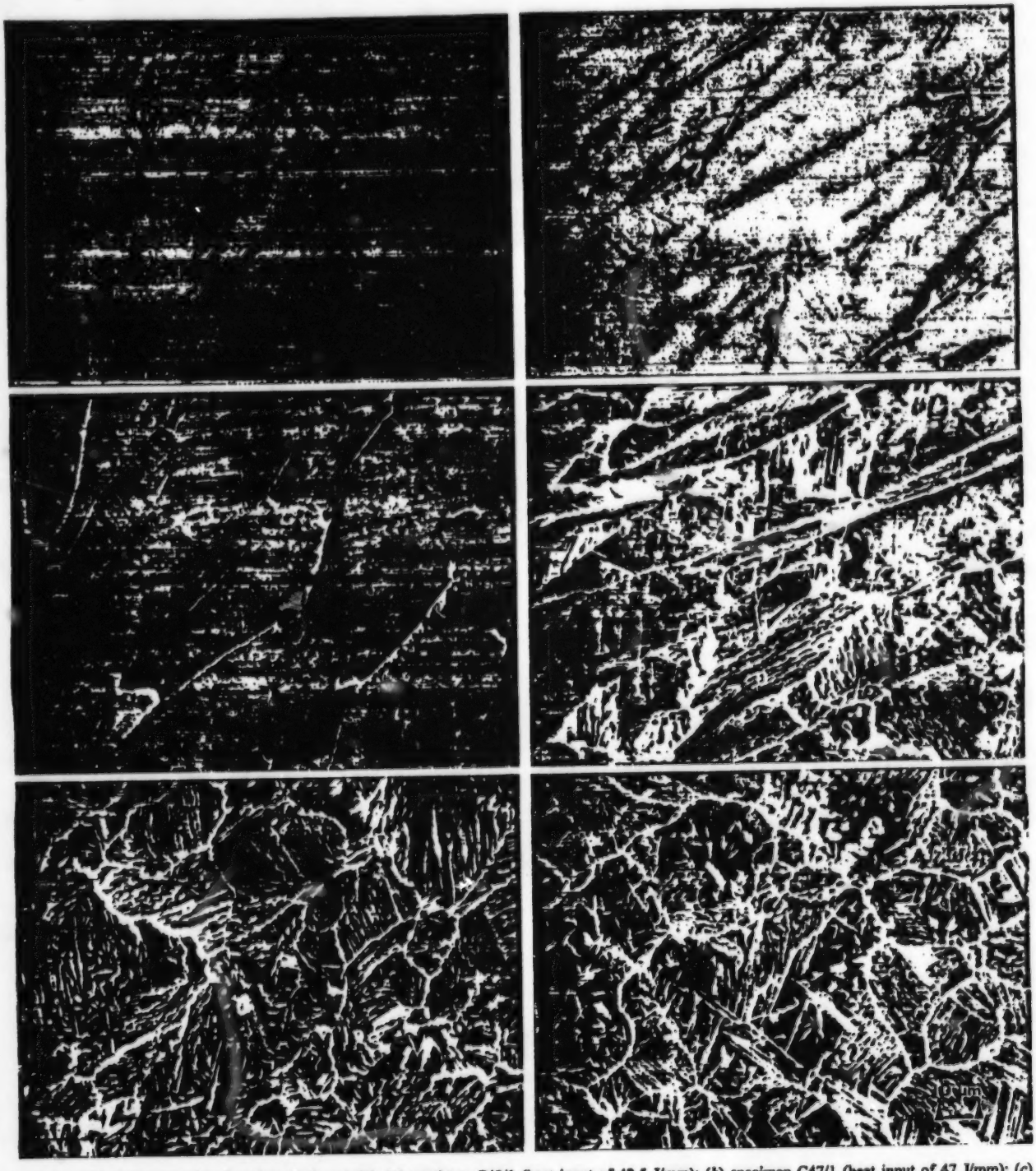

Fig. 5—Optical micrographs of as-deposited material: (*a*) specimen C43/1 (heat input of 42.5 J/mm); (*b*) specimen C47/1 (heat input of 47 J/mm); (*c*) specimen C64/3 (heat input of 64.3 J/mm); (*d*) specimen A150/2 (heat input of 150 J/mm); (*e*) specimen A390/1 (heat input of 390 J/mm) and (*f*) specimen C595/1 (heat input of 595 J/mm).

example is shown in Figure 10(a). In all cases, the darker-etching martensite was attacked preferentially, often leaving the lighter-etching grain boundary and Widmanstätten α phases standing proud on the surface. There was no significant change in weight loss with heat input, and the measured weight losses of the clad materials were consistent with those of the base materials. However, two changes in location of pitting did occur with increases in heat input.

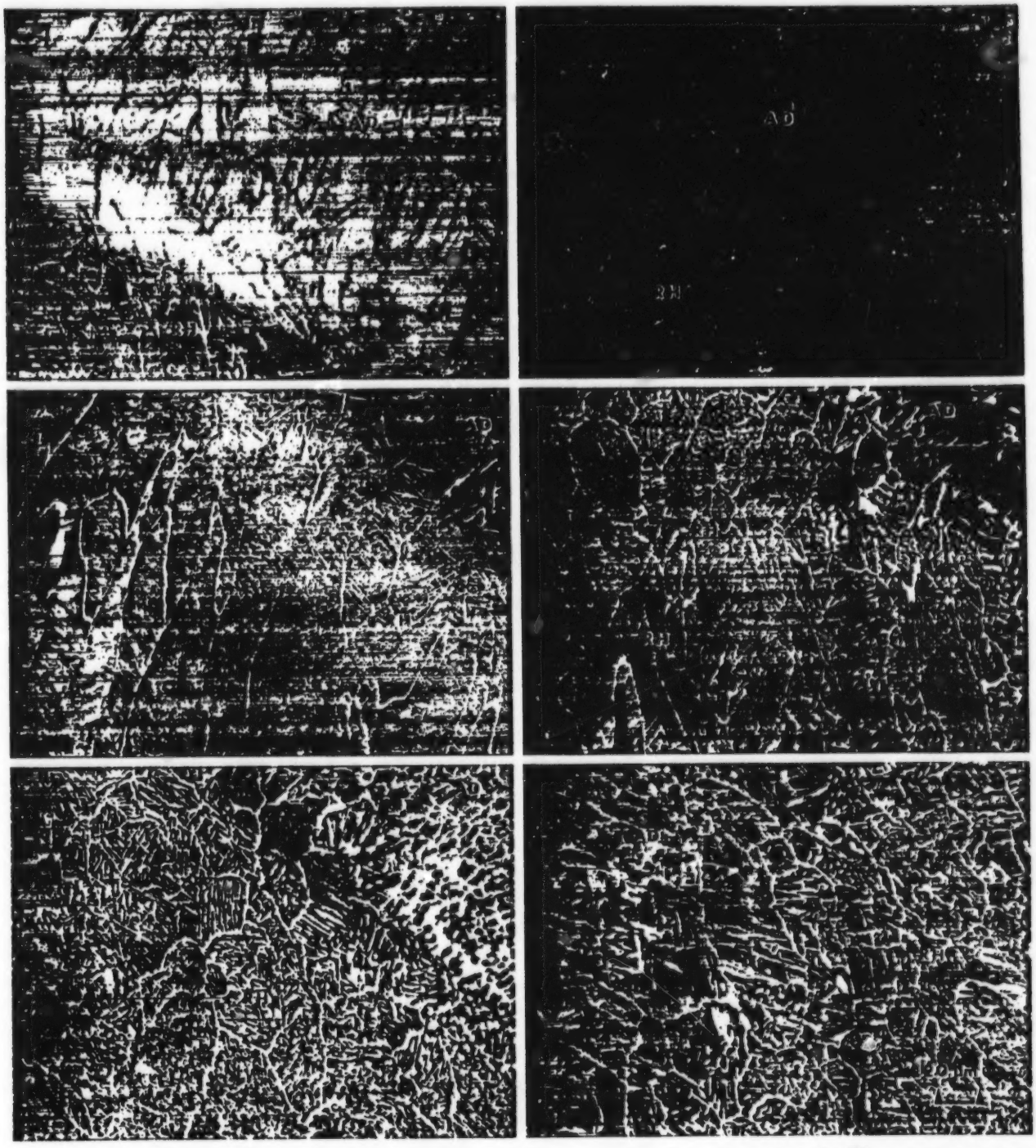

Fig. 6—Optical micrographs of reheated zone of deposit: (*a*) specimen C43/1 (heat input of 42.5 J/mm); (*b*) specimen C47/1 (heat input of 47 J/mm); (*c*) specimen C64/3 (heat input of 64.3 J/mm); (*d*) specimen A150/2 (heat input of 150 J/mm); (*e*) specimen A390/1 (heat input of 390 J/mm); and (*f*) specimen C595/2 (heat input of 595 J/mm).

First, there seemed to be an increased tendency toward pitting under the crevice in the lowest-heat-input specimen. The worst pitting seen in this work was observed in this region under the screw head on the clad face of specimen C64/2. This pitting is shown in cross section in Figure 10(b). Its depth is approximately 0.1 mm. It is interesting to note that similar pitting was also seen under the crevice of a specimen of surface-melted (*i.e.*, autogenously welded)

Table IV. Corrosion Potentials and Currents

Specimen	Heat Input (J/mm)	Corrosion Potential *vs* SCE at 23 °C (mV) Individual Test	Corrosion Potential *vs* SCE at 23 °C (mV) Average	Corrosion Current (μA/cm^2)
Alloy A 1	NA*	−346	—	0.46
Alloy A 2	NA	−337	—	0.4
Alloy A 3	NA	−332	−338 ± 8	0.25
A68/1 1	68	−362	—	0.014
A68/1 2	68	−345	−353 ± 9	0.048
A390/1 1	390	−342	—	pitting
A390/1 2	390	−361	−351 ± 10	0.16

*NA—not applicable.

UNS C95800 exposed together with the clad specimens discussed in this article. This specimen had been produced with a heat input of 20 J/mm.[21] Its composition was Cu-9.1Al-4.4Ni-3.8Fe-1.2Mn, nearly identical to that of the welding consumable used in this work. These results suggest that surfaces produced with very low heat inputs are more susceptible to crevice effects, although more work is required to understand these observations. It is also possible that these specimens exhibited a greater tendency toward crevice corrosion because all welding oxides were not removed prior to immersion. The second change in location of pitting with heat input was that only in the highest-heat-input specimen (390 J/mm—specimen A390/1) tested did pitting occur at the reheated zone in addition to in the deposit. This is shown in Figure 10(c). The presence of an equiaxed α plus martensite region in the reheated zone just adjacent to the fusion zone of the higher-heat-input specimens does not seem to have played a role in causing pitting to occur here.

On all specimens, the interface between the clad deposit and the base material was exposed to seawater, although in a number of cases, marine growth created a crevice on top of this area. In none of the specimens examined was there significant preferential attack of this region. An example of the appearance of this region after testing is shown in Figure 10(d).

A laser-clad specimen of type A150/2, immersed with the clad surface covered by a nylon pad, had a slightly more coppery surface appearance but was otherwise similar to the specimen of type A150/2 which was exposed without a pad. A specimen of type A150/2 immersed bolted to a titanium block, with the clad face up, exhibited similar, although slightly more, pitting than an uncoupled specimen. A specimen of type A150/2 immersed bolted with its clad face against a titanium block also exhibited more pitting. However, in this case, pitting occurred at the reheated zone as well.

In general, the behavior of the clad materials in the long-term exposure tests are superior or similar to that of the base alloy A, the only base alloy for which a large number of specimens were available. Alloy A was prepared as a 15.2-cm-diameter by 30.5-cm-long sand casting and, thus, had a coarse structure. When exposed uncoupled and without a nylon cap, alloy A exhibited maximum pitting, or preferential corrosion of between 40 and 100 μm. An example is shown in Figure 10(e). These are higher than the values observed for the specimens of type A150/2 and A390/1 and comparable to the one severe pit found on alloy C64/2. Adding a nylon cap worsened the amount of pitting only slightly on both specimen A150/2 and the untreated alloy A. This result can be rationalized on the basis that even the uncoupled specimens had similar crevices created by the presence of marine growth. It was in the case of titanium alloy coupling that the worst results were observed. Titanium-coupled alloy A had extensive 100-μm-deep pits and was the most severely attacked type of specimen in this work, as shown in Figure 10(f), while, as discussed in the previous paragraph, titanium-coupled specimens of type A150/2 behaved only slightly worse than the equivalent uncoupled specimens, whether they were exposed clad face toward or away from the titanium block.

E. *Bend Tests*

The bend tests showed that the clad material was much less ductile than the unclad material. When tests were conducted so that the clad surface was in tension, cracking did not occur at a bend radius of 28.7 mm but did occur at a radius of 25.4 mm. When tests were conducted so that the unclad surface was in tension, cracking did not occur at a bend radius of 9.6 mm but did occur at a bend radius of 6.4 mm. There were also differences in how cracking occurred on the two faces. Cracks on the clad specimens were audible and traveled across the whole clad face, while cracks on unclad specimens were not audible and were less extensive. The results show that the clad surface has a lower toughness than the base material.

F. *Stress Corrosion Cracking Resistance*

Three stress corrosion cracking specimens were removed from the seawater immersion tank after 1 month. Despite stresses in excess of the yield strength of the base material, no evidence of stress corrosion cracking was noted on either the treated or the untreated tine. In none of the nine stress corrosion specimens examined was evidence of cracking found by visual or die-penetrant inspection. Three of the specimens had developed severe pitting. Each of the pitted specimens had been exposed to stagnant Halifax Harbor seawater. Pitting occurred on both the clad and unclad faces, usually under a green deposit. This deposit, when dry, contained significant amounts of copper and chlorine, lesser amounts (5 to 15 pct by weight) of iron and aluminum, and trace amounts (less than 1 pct by weight) of sulfur and calcium. Powder X-ray diffraction showed that the copper hydroxychlorides Cu(OH)Cl, $Cu_3(OH)_2Cl_4$, $Cu_3(OH)_2Cl_4{\cdot}2H_2O$, and $Cu_{11}(OH)_{14}Cl_8{\cdot}6H_2O$ were present in the deposit. A number of different surface finishes were investigated in this work. It is significant that pitting did not develop on areas of the clad surface which had been ground, but only on regions which had the high-temperature oxide on the surface intact.

IV. DISCUSSION

The results of this work show that, except for a significant reduction in ductility, laser cladding either improved or did not measurably degrade the properties assessed in this work. It also showed that microstructure was strongly

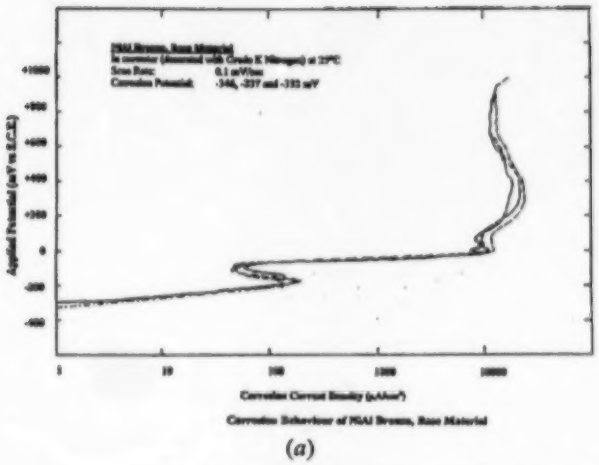

(*a*)

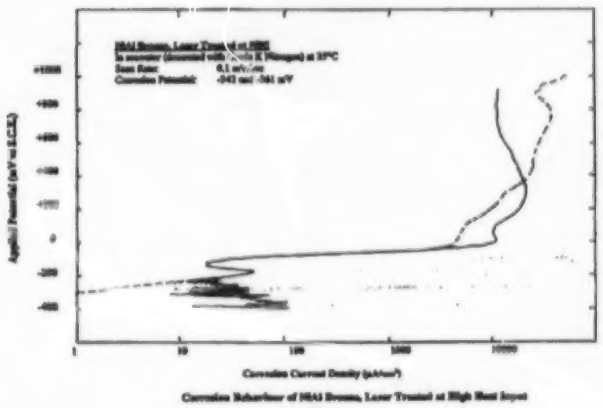

(*c*)

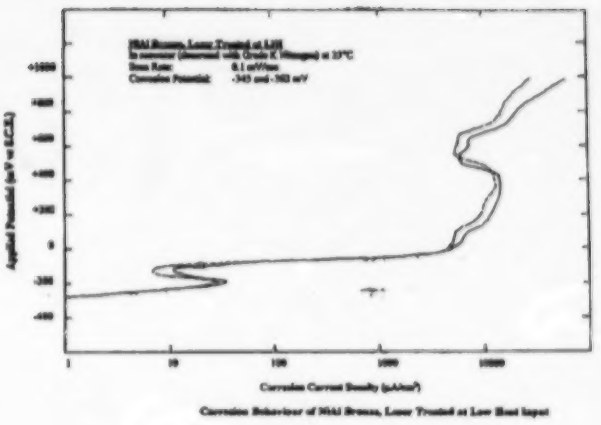

(*b*)

Fig. 7—Corrosion behavior of nickel aluminum bronze: (*a*) as-received alloy A; (*b*) specimen of type A68/1 (heat input of 68 J/mm); and (*c*) specimen of type A390/1 (heat input of 390 J/mm).

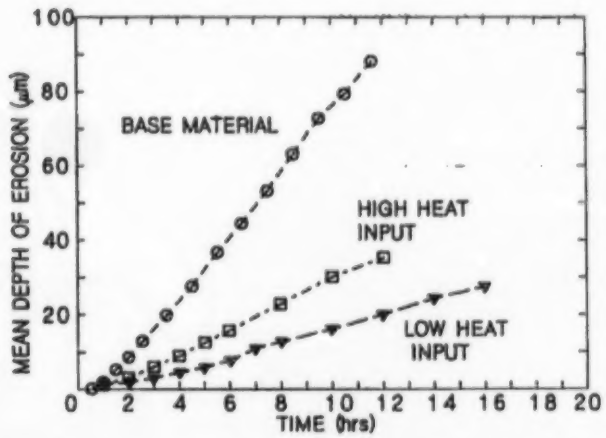

Fig. 8—Cavitation-erosion behavior of as-received alloy A (labeled base material) and clad specimens of types A390/1 (labeled high heat input) and A68/1 (labeled low heat input).

dependent on heat input. This was especially true in the as-deposited region. The reheated zone microstructure and hardness seemed to be less sensitive to heat input.

The different microstructures produced by different heat inputs had different properties. We surmise that the observation

Table V. Summary of Cavitation-Erosion Test Results

Specimen	Heat Input (J/mm)	Maximum Erosion Rate (μm/h)	Incubation Time (Min)
Alloy A	NA	7.6	69
A68/1	68	1.5	114
A390/1	390	3.0	70

of a peak deposit hardness at a heat input of 62.5 J/mm is the result of precipitation hardening. The order of cavitation-erosion resistance observed in this work was laser-clad at 68 J/mm > laser-clad at 390 J/mm > base material.

This is the same order as the average material hardness, although the differences in ductility of the base and laser-clad material did not make the observed order of cavitation resistance predictable. It is intriguing that the base material and the higher-heat-input clad material have the same incubation time, while the higher-heat-input clad material is more resistant to cavitation-erosion. In contrast, the low-heat-input case had a longer incubation time than the base material and an improved resistance to cavitation-erosion. It has long been noted that there is a relationship between corrosion-fatigue limit and incubation time,[2] so, at least for the low-heat-input case, an increase in the corrosion-fatigue limit might be expected. The observed localization

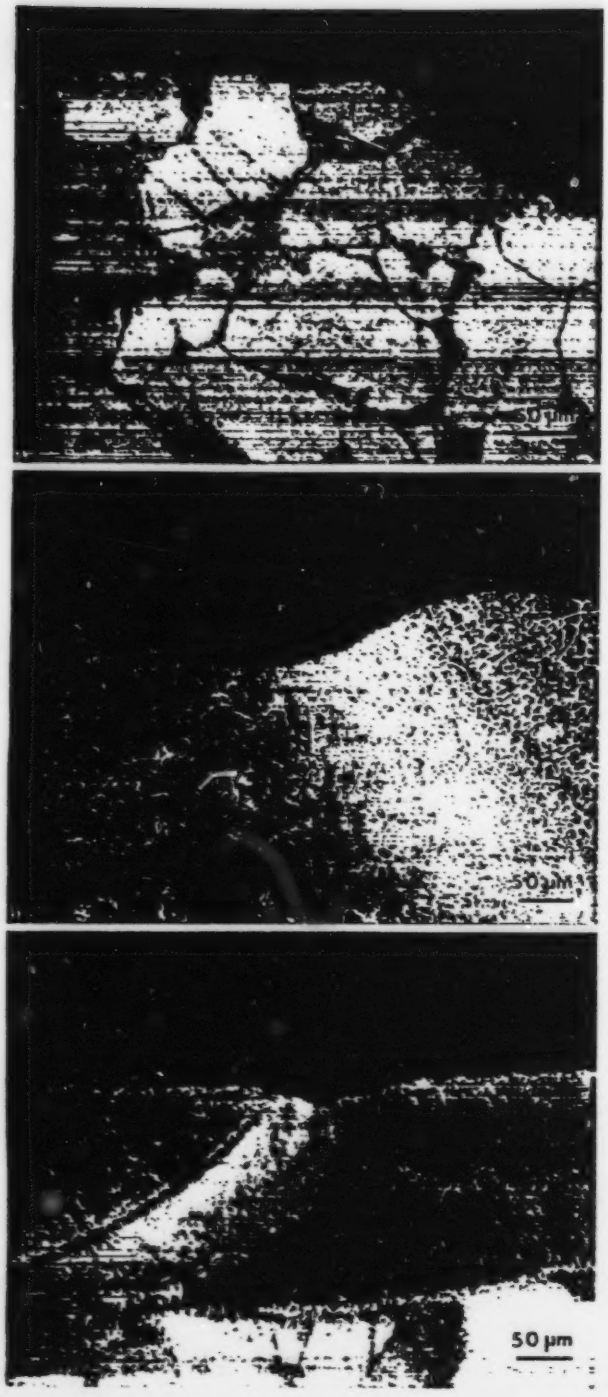

Fig. 9—Optical micrographs of cavitation erosion specimens: (*a*) as-received alloy A; (*b*) specimen of type A390/1 (labeled high heat input in Fig. 8); and (*c*) specimen of type A68/1 (labeled low heat input in Fig. 8).

of cavitation-erosion attack at the reheated zones of the laser-clad specimens may affect the validity of the correlation just mentioned and may have implications for in-service interaction between corrosion-fatigue and cavitation-erosion. For both clad conditions subjected to cavitation-erosion testing, an improvement in corrosion fatigue life in the so-called mortal zone is also expected, based on published relationships between cavitation-erosion data and mechanical properties.[40]

The low-heat-input deposit microstructure, which favored cavitation resistance, seemed to be more prone to pitting in the long-term corrosion experiments than the higher-heat-input deposits. It is interesting that only at higher heat inputs did pitting of heat-affected zones occur. It is also interesting that only in the higher-heat-input case did the potentiodynamic corrosion studies suggest a tendency to pitting. The presence of oxide from welding seemed to be associated with much, and perhaps all, of the pitting observed. Explanation of these phenomena requires more detailed metallographic and electrochemical studies, but is an important part of optimizing deposit processing and composition to give optimum properties.

The results in this article are for a commercially available consumable composition. While improvements in properties over the bulk occur over a wide range of heat inputs, both structure and properties were highly dependent upon heat input. Comparing the results of this study to work with a consumable of composition Cu-10.6Al-5.1Ni-1.3Mn shows that both the peak hardness and the heat input at which the peak hardness is achieved are functions of heat input.[41] Thus, to reduce the sensitivity to heat input, and to make greater property improvements, the effect of the consumable composition needs to be examined and the consumable composition needs to be optimized. In terms of microstructure, the goals of such an approach should be to make the as-deposited material microstructure less sensitive to heat input and to make the microstructure and hardness of the reheated material similar to that of the as-deposited material. In terms of properties, the goals should be to increase ductility and avoid pitting sensitivity in either the as-deposited or the reheated material, while retaining or improving upon increases in resistance to cavitation-erosion and general corrosion.

V. CONCLUSIONS

The microstructures of both the as-deposited and reheated material in a laser-clad deposit produced using a welding wire of composition Cu-9.0Al-4.6Ni-3.9Fe-1.2Mn were sensitive to heat input. At the lowest heat input investigated (42.5 J/mm), the as-deposited material had a predominately martensitic microstructure, although a few prior β boundaries were outlined with grain boundary allotriomorphic α. As heat input increased, the fraction of prior β grain boundaries which were outlined with α increased. At a heat input of 47.2 J/mm, secondary Widmanstätten α began to form. The amount of secondary Widmanstätten α precipitation increased with heat input. By a heat input of 150 J/mm, primary intragranular Widmanstätten α had begun to form in the as-deposited material as well. The amount and coarseness of Widmanstätten α precipitation increased with heat input. The hardness of the as-deposited material reached a maximum at a heat input of 64 J/mm, probably because of a secondary precipitation-hardening effect.

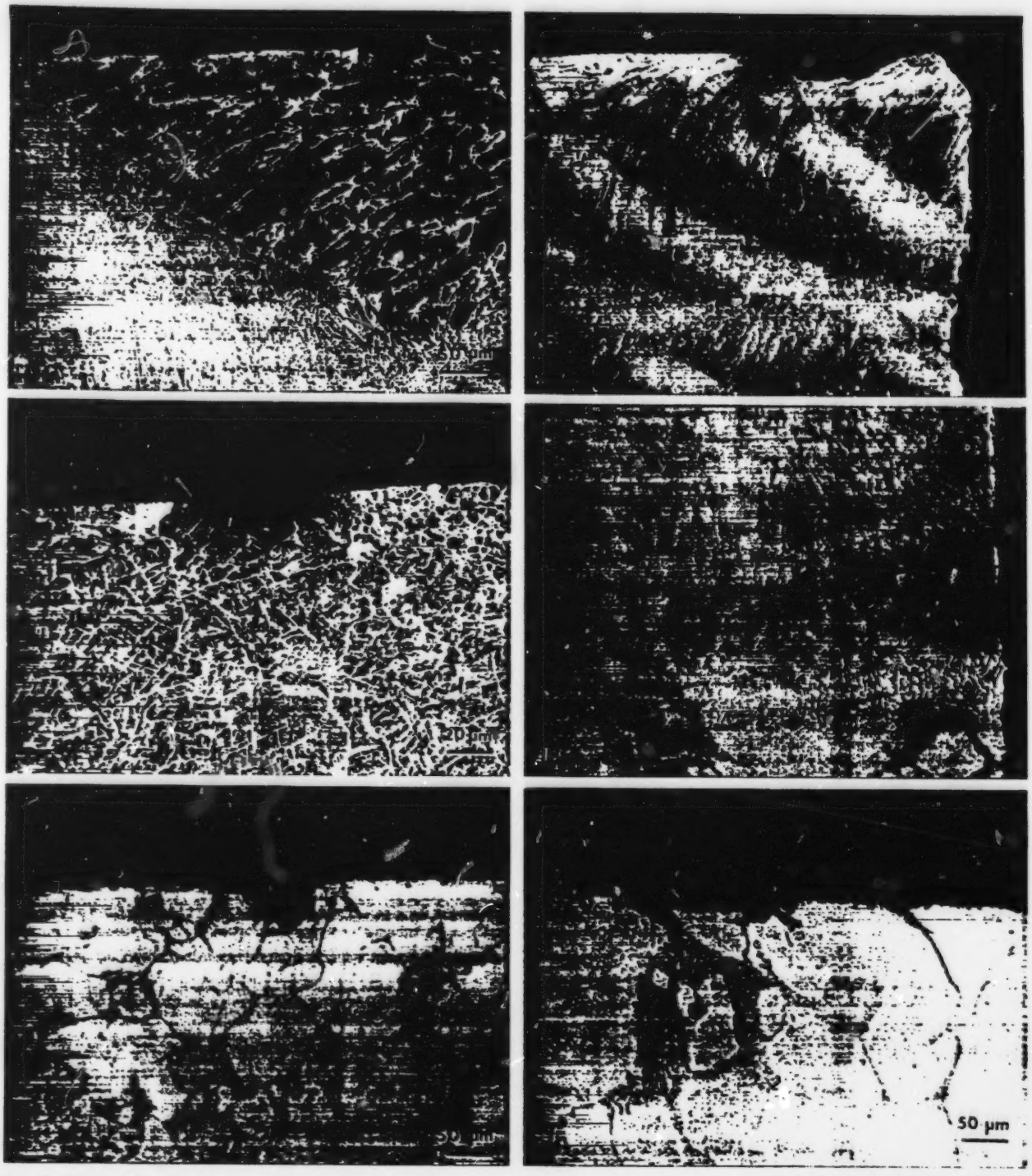

Fig. 10—Micrographs of long-term corrosion specimens: (*a*) specimen of type A150/2 exposed coupled to Ti; (*b*) specimen of type C64/2, in region under nylon screw head; (*c*) specimen of type A390/1, showing small pit in heat-affected zone; (*d*) surface where deposit meets base material on a specimen of type A150/2 exposed coupled to Ti; (*e*) as-received alloy A exposed uncoupled; and (*f*) as-received alloy A exposed coupled to Ti-6Al-4V.

Over the range of heat inputs investigated in this work, the reheated zone always contained Widmanstätten and grain boundary α. As well, the minimum hardness of the reheated zones was always below HV 300, regardless of heat input.

The properties of the deposit also depended strongly on

heat input. Cavitation-erosion resistance was higher in a specimen produced at lower heat input, and the location where pitting occurred seems to depend on heat input. Of the properties investigated, only ductility was adversely affected by laser cladding. Most properties were improved.

ACKNOWLEDGMENTS

The technical assistance of Messrs. Bob Armstrong and Bob Johnson is gratefully acknowledged.

REFERENCES

1. P.J. Macken and A.A. Smith: *The Aluminum Bronzes, Properties and Production Processes*, CDA Publication 31, CDA, Herts, England, 1966.
2. F.L. LaQue: *Marine Corr.*, Wiley, New York, NY, 1975.
3. *Rules for Building and Classing Steel Vessels*, American Bureau of Shipping, Paramus, NJ, 1990, sect. 37/2.
4. *Rules and Regulations for the Classification of Shipping*, Lloyds Resister of Shipping, London, 1978, part 5, ch. 7, sects. 2.1 and 3.1 and part 2, ch. 9, sect. 1.
5. C.F. Zanis and R.J. Ferrara: *AFS Trans.*, 1974, vol. 53, pp. 71-78.
6. J.C. Rowlands: *Proc. 8th Int. Congr. on Metallic Corrosion*, Mainz, Germany, 1981, pp. 1346-51.
7. R.J. Ferrara and T.E Caton: *Materials Performance*, February, 1982, pp. 30-34.
8. E.A. Culpan and G. Kose: *Br. Corr. J.*, 1979, vol. 14, pp. 160-66.
9. P. Brezina: *Int. Met. Rev.*, 1982, vol. 27, pp. 77-120.
10. C.W. Draper: *Lasers in Metallurgy*, TMS, Warrendale, PA, 1981, pp. 21-31.
11. C.W. Draper: *J. Mater. Sci.*, 1981, vol. 16, pp. 2774-80.
12. C.W. Draper, J.M. Vandenberg, C.M. Preece, and C.R. Clayton: *Rapidly Solidified Amorphous and Crystalline Alloys*, Elsevier, New York, NY, 1982, pp. 529-33.
13. C.W. Draper and S.P. Sharma: *Thin Solid Films*, 1981, vol. 84, pp. 333-40.
14. C.W. Draper, S.P. Sharma, J.L. Yeh, and S.L. Bernasek: *Surf. Interface Analysis*, 1980, vol. 2, pp. 179-82.
15. R.J. Taylor, D.A. Weston, G.M. Wright, and B.W. Turnbull: *Corr. Australasia*, 1981, Sept., pp. 12-17.
16. N. Dubnyakov, I.B. Malysheva, and S.F. Pulim: *Sov. J. Friction Wear*, Allerton Press, New York, NY, [1986, vol. 7,] pp. 70-76 (translation).
17. F. Hasan, A. Jahanafrooz, G.W. Lorimar, and N. Ridley: *Metall. Trans. A*, 1982, vol. 13A, pp. 1337-45.
18. Y. Liu, J. Mazumder, and K. Shibata: *Metall. Mater. Trans. A*, 1994, vol. 25A, pp. 37-46.
19. Y. Liu, M.E. Mochel, J. Mazumder, and K. Shibata: *Acta Metall.*, 1994, vol. 42, pp. 1763-68.
20. Y. Liu, J. Mazumder, and K. Shibata: *Metall. Mater. Trans. B*, 1994, vol. 25B, pp. 749-59.
21. C.V. Hyatt, K.H. Magee, J. Hewitt, and T. Betancourt: *Abstracts and Summaries of the 2nd CF/CRAD Meeting on Naval Applications of Materials Technology*, J.R. Matthews, ed., Defence Research Establishment Atlantic, Dartmouth, NS, Canada, pp. 226-52.
22. C.V. Hyatt and K.H. Magee: *Proc. Advanced Methods of Joining New Materials II*, The American Welding Society, Miami, FL, 1994, pp. 111-26.
23. D.E. Bell: Master's Thesis, The Pennsylvania State University, University Park, PA, 1993.
24. K. Petrolonis: Master's Thesis, The Pennsylvania State University, University Park, PA, 1993.
25. P.J. Oakley and N. Bailey: *Proc. Int. Conf. on Power Beam Technology*, The Welding Institute, Cambridge, United Kingdom, 1986, pp. 301-14.
26. F. Hansan, G.W. Lorimar, and N. Ridley: *Proc. Conf. on Phase Transformations*, Cambridge, United Kingdom, 1987, pp. 131-34.
27. D.E. Bell, K. Petrolonis, and P.R. Howell: *Proc. Int. Trends in Welding Science and Technology*, S.A. David and J.M. Vitek, eds., Gatlinburg, TN, pp. 301-05.
28. D.E. Bell, T.A. Marsico, K. Petrolonis, P.E. Denney, and P.R. Howell: in *Metallography: Past, Present and Future*, ASTM STP 1165, G.F. Vander Voort, F.J. Warmoth, S.M. Purdy, and A. Szirmae, eds., ASTM, Philadelphia, PA, 1995, pp. 327-434.
29. J.A. Gianetto, M. Sahoo, M.W. Letts, and C. Bibby: "The Microstructural Characterization of NiAl Bronze Weldments," DREA CR/95/435, Defence Research Establishment Atlantic, Dartmouth, NS, Canada, 1995.
30. C.V. Hyatt: "Review of Literature Related to Microstructural Development during Laser Surface Engineering of Nickel Aluminum Bronze," DREA Technical Memorandum TM/96/227, Defence Research Establishment Atlantic, Dartmouth, NS, Canada, 1996.
31. J.C. Bennett and C.V. Hyatt: *Proc. Micros. Soc. Canada*, vol. 24, 1997, pp. 70-71.
32. V. Merchant, C.V. Hyatt, D.O. Morehouse, and J. Hewitt: Defence Research Establishment Atlantic, Dartmouth, Nova Scotia, Canada B2Y 3Z7, unpublished research, 1995.
33. *Standard Reference Test Method for Making Potentiostatic and Potentiodynamic Anodic Polarization Measurements*, ASTM Standard G5-87, *1987 Annual Book of ASTM Standards*, ASTM, Philadelphia, PA, vol. 03.02, pp. 124-31.
34. *Standard Method of Vibratory Cavitation Erosion Test*, ASTM Standard G32-85, *1987 Annual Book of ASTM Standards*, ASTM, Philadelphia, PA, vol. 03.02, pp. 187-94.
35. *Standard Method for Conducting Corrosion Coupon Tests in Plant Equipment*, ASTM Standard G4-87, *1987 Annual Book of ASTM Standards*, ASTM, Philadelphia, PA, vol. 03.02, pp. 111-23.
36. *A Standard test Method for Semi-Guided Bend Test for Ductility of Metallic Materials*, ASTM Standard E 290-87, *1987 Annual Book of ASTM Standards*, ASTM, Philadelphia, PA, vol. 03.01, pp. 577-81.
37. *Standard Practice for Preparation of Stress Corrosion Test Specimens for Weldments, ASTM Standard G58-85, 1987 Annual Book of ASTM Standards*, ASTM, Philadelphia, PA, vol. 03.02, pp. 326-34.
38. A.W. Loginow and E.H. Phelps: *Corrosion*, 1962, vol. 18, pp. 299t-305t.
39. S.D. Antolovich: *Metals Handbook*, vol. 19, *Fatigue and Fracture*, ASM, Materials Park, OH, 1996, pp. 27-41.
40. R.H. Richman and W.P. McNaughton: *Wear*, 1990, vol. 140, pp. 69-83.
41. K.H. Magee: "Laser Cladding of Marine Copper Alloys," DREA CR/94/424, Defence Research Establishment Atlantic, Dartmouth, NS, Canada, 1994.

#509920